Low-field transport measurements in superconducting Co/Nb/Co trilayers

G. Carapella,* F. Russo, and G. Costabile
CNR-INFM "SUPERMAT" and Dipartimento di Matematica e Informatica, Universitá di Salerno, via Ponte don Melillo, I-84084 Fisciano, Italy

(Received 18 April 2008; revised manuscript received 27 July 2008; published 30 September 2008)

We report transport measurements in a superconducting Co/Nb/Co trilayer based on elemental ferromagnetic Co and elemental superconducting Nb. The trilayer behaves as a superconducting valve, can be operated at liquid-helium temperature, and can switch from superconductive to normal state in weak applied in-plane magnetic fields. Current-voltage curves, critical currents as a function of temperature and magnetic field, as well as preparation of superconductive or resistive state are addressed here. Data analysis suggests that the superconducting valve behavior can be accounted for by a glassy vortex phase induced in the superconductor by the stray fields from domain walls proliferating around the coercive fields of the ferromagnetic electrodes.

DOI: 10.1103/PhysRevB.78.104529 PACS number(s): 74.78.−w, 74.25.Qt, 74.25.Fy, 85.75.−d

I. INTRODUCTION

In a ferromagnet/superconductor/ferromagnet (FSF) trilayer, superconductivity can be controlled by the relative orientation of the magnetizations of the outer ferromagnetic electrodes sandwiching the superconductor. In other words, FSF trilayers can act as a spin switch. The possibility to control superconductivity by means of a relatively weak magnetic field in such a way was proposed long time ago by de Gennes.[1] In the pioneering experiments, superconductivity was found to be depressed for parallel alignment of in-plane magnetizations of the outer ferromagnetic insulators[2] or weakly coupled (a very thin insulating barrier at SF interfaces) metallic ferromagnets.[3] Recently, spin switches based on proximity coupled metallic ferromagnets[4,5] and low-T_c superconductors[6–14] or high-T_c superconductors and manganites[15] have been widely investigated. The experimental results suggest that superconductivity can be depressed both in the parallel ($|\mathrm{P}\rangle$) state of the magnetizations[6–8] (standard spin switch effect) and in the antiparallel ($|\mathrm{AP}\rangle$) state[9–15] (inverse spin switch effect). The individuation of the main mechanism of magnetoquenching of superconductivity in FSF trilayers is again a hot topic of discussion.[12] While observed[6–8] standard spin switch effect has been reliably ascribed to the mechanisms of pair breaking induced by exchange field,[4,5] the inverse spin switch effect has been ascribed to the quasiparticle spin imbalance[16] in some experiments[9–11,15] and to stray field from domain walls in other experiments.[12–14]

Most of the experiments reported in the literature focused on the individuation of two critical temperatures corresponding to the $|\mathrm{AP}\rangle$ or $|\mathrm{P}\rangle$ state of the FSF trilayer. Apart from some exception,[13,14] no particular emphasis has been given to the transport properties of the trilayers. Here, beside the use of a combination of materials not yet tested as Nb and Co, we report an experimental study that addresses more specifically these properties to gain experimental information also from a different point of view. In particular, we report an analysis of the current-voltage curves and the critical currents as a function of magnetic field and temperature: a topic not addressed in detail in the literature. Also, in view of possible applications of the FSF trilayer, we try out the preparation of superconductive or resistive state at liquid-helium temperature. We show here that this is reliably achieved using suitable sense currents. Our Co/Nb/Co trilayer was realized in a pseudospin valve configuration; i.e., the bottom and top Co layers were deposited with different thicknesses to achieve different coercive fields. As it will be more clear in the following, we were not able to accomplish well-defined $|\mathrm{AP}\rangle$ and $|\mathrm{P}\rangle$ states between the coercive fields of our structure as such states were affected by a significant domain component. Therefore, we name such states $|\mathrm{AD}\rangle$ and $|\mathrm{PD}\rangle$ to remark that we are concerned with not fully saturated magnetizations between coercive fields. Such a situation is similar to the one reported[12–14] for other FSF trilayers where the pseudospin valve configuration was tried. Nevertheless, the device exhibited a superconducting valve behavior with superconductivity suppressed in the $|\mathrm{AD}\rangle$ state resembling inverse spin switch effect. Data analysis suggests that in our Co/Nb/Co structure, with films having macroscopic lateral size, the valve operation can be ascribed to the mechanisms[12–14] of depression of superconductivity due to stray fields originating from domain walls. The vortex matter induced in the superconductor seems to be consistent with the occurrence of a glassy vortex phase.

II. EXPERIMENTS

The Co/Nb/Co trilayers were deposited onto glass substrates by rf magnetron sputtering in a high-vacuum system with a base pressure of 2×10^{-7} Torr in 99.999% pure Argon at 3.1×10^{-3} Torr at room temperature. Co was deposited at the rate of 0.1 nm/s producing a roughness smaller than 0.5 nm. The Nb was deposited with the rate of 2.2 nm/s producing a roughness below 1.5 nm. The roughness of Nb and Co films was measured by an atomic force microscopy (AFM) on a $1\times\mu\mathrm{m}^2$ area. The grade of contamination of sputtered films was checked by energy dispersive spectroscopy (EDS) analysis giving no measurable traces other than the ones present on target materials (Co 99.95% pure and Nb 99.98% pure). In order to get different coercive fields, the bottom and the top Co films were deposited with different thicknesses in a pseudospin valve configuration.[9,10,12,13,15] In all the samples the bottom Co layer is 8 nm thick, the top Co

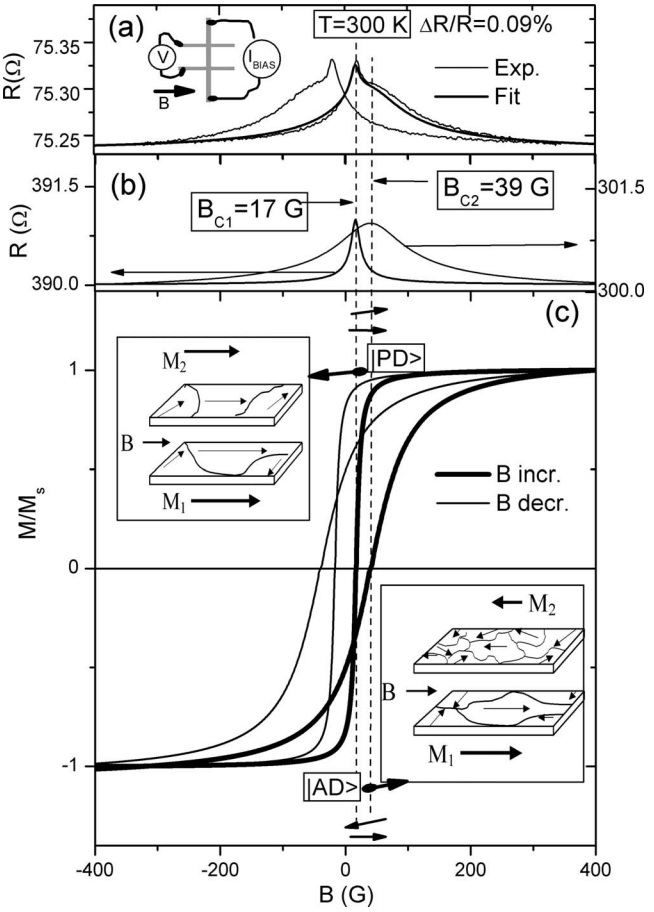

FIG. 1. (a) Magnetoresistance of the trilayer measured at room temperature for in-plane magnetic field applied as shown in the inset together with a fitting curve. (b) The trial AMR signals of the two ferromagnetic layers we used in the fit. (c) Hysteresis loops of the magnetic layers calculated from AMR signals. A schematic drawing of the magnetic configuration of the ferromagnetic layers in two significant states is given in the insets.

layer is 16 nm thick, while Nb thickness ranges from 18 to 32 nm. The trilayer is covered by a 4 nm Al cap layer to prevent the oxidation of the top layer. The Al is a good cap layer[17] as its native oxide (Al_2O_3) thermally grown in air is very compact and saturates at about 2 nm. Hence, in the following, the cap layer is intended as 2 nm Al covered by a 2 nm native oxide. The whole trilayer was patterned in a Hall geometry, as sketched in the inset of Fig. 1, that allows four contacts measurements. The width of the strips is 200 μm, and voltage contacts are 3 mm apart. All samples showed similar behavior, with a zero resistance critical temperature decreasing as Nb thickness was decreased. Here we report about a sample with 30-nm-thick Nb that allowed us to operate in a standard liquid-helium cryostat at 4.2 K.

In Fig. 1(a) we show the magnetoresistance of the trilayer measured at room temperature for in-plane magnetic-field applied as shown in the inset. The maxima in the curve are structured suggesting the presence of two coercive fields corresponding to the two magnetic layers of different thickness. Structured minima or maxima pointing to the presence of two coercive fields are obtained also for magnetic field oriented parallel to the current or in a planar Hall-effect (PHE) configuration. Noticing that the spacer layer is very thick, we can assume the total magnetoresistance signal as originating from a parallel connection of magnetic-field-dependent anisotropic magnetoresistance (AMR) signals of the two magnetic layers and magnetic-field-independent resistance of normal layer. The giant magnetoresistance (GMR) contribution can be neglected due to the vanishingly small $\Delta R/R \approx 0.09\%$ we observe. In Fig. 1(b) we show a combination of AMR signals that combined with normal layer resistance can account for the fit of experimental data shown in Fig. 1(a). From the two AMR, the normalized hysteresis loops of magnetic layers shown in Fig. 1(c) can be calculated.[18] For what concerns the magnetization reversal of the two ferromagnetic layers, the hysteresis loops in Fig. 1(c) suggest that for the layer with larger coercive field (that we associated to the top Co layer; see below) a domain-wall motion mechanism mixed to a magnetization rotation takes place; while for the layer with lower coercive field (bottom Co layer), a domain-wall motion prevails over rotation. Inspection of hysteresis loops also indicates that although not very well defined, an $|AP\rangle$ state for the trilayer is achieved in windows centered around $B = \pm 25$ G at room temperature. However, the rather broad signals shown in Fig. 1 suggest that both $|AP\rangle$ and $|P\rangle$ states are mixed to a substantial domain state of the ferromagnetic films; so that the two most significant states in the magnetic-field range between the coercive fields of our trilayer are an antiparallel-domain state $|AD\rangle$ and a parallel-domain state $|PD\rangle$ as sketched in the insets of Fig. 1(c). In other words, *parallel* or *antiparallel* is referred to the total (vector sum) magnetization of the ferromagnetic layers averaged on the macroscopic size of the layers. A fully saturated parallel magnetization state (both layers in a monodomain state) is obtained only for large negative or positive fields. Restricting ourselves to positive field range, the $|AD\rangle$ state is achieved between the coercive fields by increasing the magnetic field from large negative values [relevant hysteresis loop branches are the thick lines in Fig. 1(c)], and the $|PD\rangle$ state is achieved by decreasing the magnetic field from large positive values [relevant hysteresis loop branches are now the thin lines in Fig. 1(c)]. Again, as the insets in Fig. 1(c) suggest, we expect more domain walls in the $|AD\rangle$ state than in the $|PD\rangle$ state. Finally, to remember that the antiparallel and parallel states between coercive fields are not ideal, in the following we will label them with two almost antiparallel or parallel arrows, as in Fig. 1(c). Coercive fields increase when temperature is decreased so the range of the magnetic field where antiparallel-domain or parallel-domain states are achieved is expected to increase as well.

In Fig. 2(a) we show the curve of the voltage (at constant bias current) versus magnetic field at a temperature slightly larger than the zero resistance critical temperature. The magnetic field is applied in the plane of the trilayer and directed as shown in the inset of Fig. 1(a). In the inset of Fig. 2(b) we show the current-voltage curve of the trilayer at a temperature lower than T_c and at zero applied magnetic field. As it is seen, a critical current I_c can be identified. At this temperature, biasing the device with a current slightly larger than I_c or approximately equal to I_c, the voltage versus field curves shown in Figs. 2(b) and 2(c) are recorded. The magnetore-

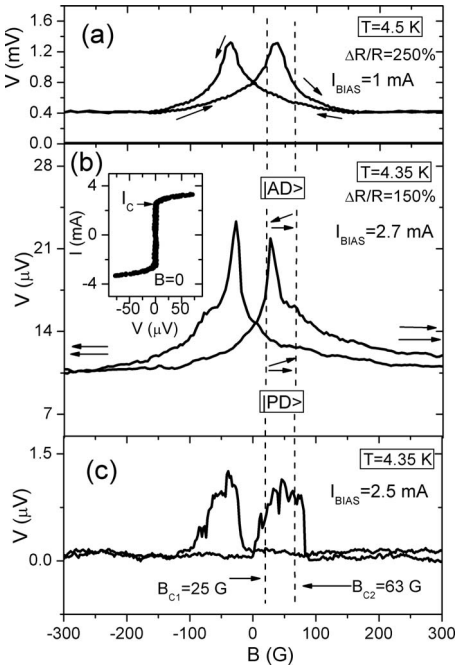

FIG. 2. (a) Voltage versus field at constant bias current of the trilayer at a temperature slightly larger than T_c for in-plane magnetic field applied perpendicularly to the bias current direction. The arrows show the direction of the field sweep. (b) Voltage versus field at a temperature lower than T_c with bias current fixed at a value slightly larger than the critical current at zero field. The current-voltage curve at zero applied field is shown in the inset. The arrows show the possible magnetic configuration of the outer ferromagnetic electrodes in the relevant magnetic-field ranges. (c) Same as in (b) but with bias current fixed at a value that is very close to the critical current in zero field.

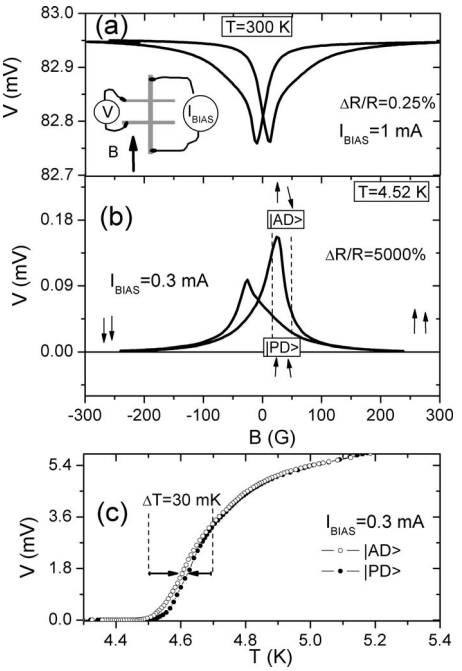

FIG. 3. (a) Voltage at constant current versus field of the trilayer at room temperature. The in-plane magnetic field is applied parallel to the current. (b) Same as in (a) but at a temperature slightly larger than T_c. (c) Voltage at constant current versus temperature of the trilayer prepared in the $|\mathrm{PD}\rangle$ or $|\mathrm{AD}\rangle$ state.

sistance ratio $\Delta R/R$ is found to be very large and diverging [as can be deduced from Fig. 2(c)] for suitably chosen bias current. At temperatures where the Nb is normal (above 5 K), the magnetoresistance curves (not shown) exhibit peaks of resistance approximately at same locations as in Fig. 2. We notice that voltage-field curve in Fig. 2(b) qualitatively resembles the room-temperature magnetoresistance shown in Fig. 1(a), allowing us to identify again two coercive fields as shown in Fig. 2(c). Coherently with the decoupled pseudo spin valve behavior in the normal state and with the discussion of Fig. 1, we can expect that relative orientations for magnetizations of outer electrodes as shown by the arrows in Fig. 2(b) have the same meaning as the ones in Fig. 1(c); i.e., they label $|\mathrm{AD}\rangle$ and $|\mathrm{PD}\rangle$ states. A fully saturated parallel-monodomain state for magnetizations is only attained at large positive or negative fields as sketched in Fig. 2(b). Resistance is found to be larger in the $|\mathrm{AD}\rangle$ state, i.e., a behavior close to the inverse spin switch effect is exhibited by the Co/Nb/Co trilayer, in qualitative agreement with other reported FSF trilayers where the pseudo spin valve configuration[9–13,15] was used to realize the antiparallel state.

The behavior of the trilayer was found qualitatively the same also for in-plane magnetic field applied parallel to the current flow as shown in Fig. 3. The voltage versus field at room temperature in Fig. 3(a) is the AMR signal we should expect for a decoupled pseudo spin valve with field applied parallel to the current. Though less evident, structured minima pointing to the presence of two coercive fields are again present. The voltage-field curve at a temperature slightly larger than T_c is shown in Fig. 3(b). As before, a superconducting valve behavior is recovered with magneto-quenching of superconductivity in the $|\mathrm{AD}\rangle$ state achieved between the two coercive fields and a magnetoresistance ratio much larger than the one observed at room temperature. In Fig. 3(c) we show curves of the voltage at constant current (proportional to resistance) versus temperature for two values of the magnetic field that induce an $|\mathrm{AD}\rangle$ or a $|\mathrm{PD}\rangle$ state for magnetizations. A $\Delta T=30$ mK in the middle of transition is observed.

V-T curves for magnetic field applied perpendicular to the current are shown in Fig. 4(a). Here the bias current is smaller than in Fig. 3(c) and a slightly larger T_c is measured as we should expect. A $\Delta T=30$ mK in the middle of transition is again observed. As it is seen from the inset, there is a small temperature range where the $|\mathrm{PD}\rangle$ state is superconducting ($V=0$) and the $|\mathrm{AD}\rangle$ state is resistive. We found no significant qualitative differences in the trilayer behavior for field applied parallel or perpendicular to the current. Therefore in the following discussion we shall consider that the magnetic field is always applied perpendicular to the current. The current-voltage curves of the superconducting valve prepared in the $|\mathrm{PD}\rangle$ or $|\mathrm{AD}\rangle$ state recorded at liquid-helium temperature are shown in the inset of Fig. 4(b) together with the identification of the two critical currents $I_c^{|\mathrm{PD}\rangle}$ and $I_c^{|\mathrm{AD}\rangle}$ at this temperature. From the data we estimate a critical current density in the parallel-domain state at 4.2 K $J_c^{|\mathrm{PD}\rangle} \simeq 2$

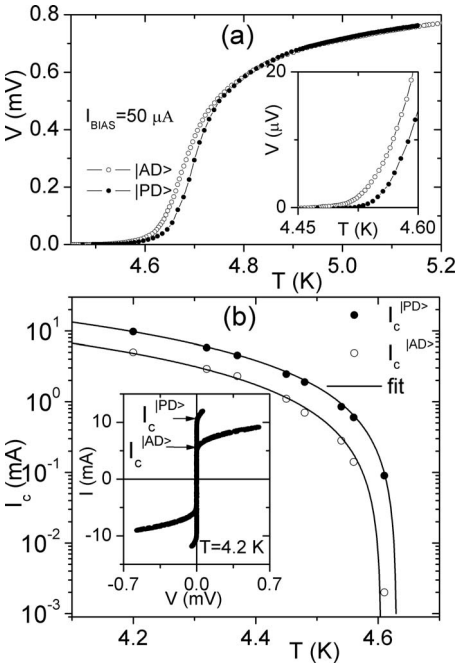

FIG. 4. (a) Voltage at constant current versus temperature of the trilayer prepared in the two states. The field is applied perpendicularly to the current. The inset shows an enlargement of the curves around the transition temperatures. (b) Critical current versus temperature in the $|\mathrm{PD}\rangle$ or $|\mathrm{AD}\rangle$ state. The solid line is a fit with theory. In the inset it is shown the $I(V)$ of the trilayer prepared in the two states recorded at 4.2 K.

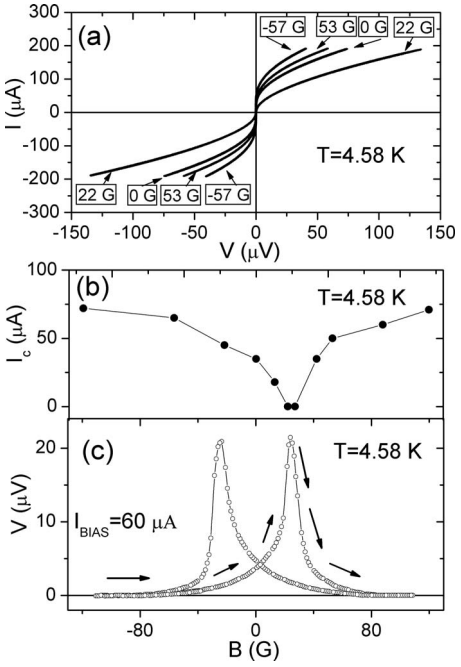

FIG. 5. (a) Current-voltage curves of the device as the magnetic field is increased from negative to positive values. (b) Critical current versus magnetic field for field increasing from negative to positive. (c) Voltage at a fixed bias current vs magnetic field. The arrows identify the curve traced in the same magnetic-field halfloop as in (b).

$\times 10^5$ A/cm^2. The two critical currents as a function of temperature are reported in Fig. 4(b). The two currents are always appreciably different with $I_c^{|\mathrm{PD}\rangle}$ about doubling $I_c^{|\mathrm{AD}\rangle}$ at 4.2 K and also much larger than $I_c^{|\mathrm{AD}\rangle}$ near the transition temperatures. Both critical currents are adequately fitted with the formula[19] valid for isolated thin films near the transition temperature,

$$I_c^i = I_{c0}^i [1 - T/T_c^i]^{3/2},$$

where $i = |\mathrm{PD}\rangle, |\mathrm{AD}\rangle$. From the fit we estimated $T_c^{|\mathrm{PD}\rangle} = 4.63$ K and $T_c^{|\mathrm{AD}\rangle} = 4.60$ K. Moreover, the critical current densities at $T=0$ can be extrapolated as $J_{c0}^{|\mathrm{PD}\rangle} = 5.7 \times 10^6$ A/cm^2 and $J_{c0}^{|\mathrm{AD}\rangle} = 3.1 \times 10^6$ A/cm^2. So, although a weakening due to the proximity effect is unavoidable, the trilayer is found capable to operate with critical currents of almost the same order of magnitude as the critical current of the isolated superconductive film. The fact that in the magnetoquenched state, i.e., our $|\mathrm{AD}\rangle$ state, the critical current follows again a genuine thin superconducting film behavior allows us to rule out mechanisms of very localized weakening of superconductivity (e.g., the formation of an isolated weak link caused by a localized fringe field as discussed by Clinton and Johnson[20]), although we cannot exclude *a priori* a uniform distribution of local depressions (e.g., fringe fields from domain walls in the domain state[12–14]) that could also account for the observed temperature dependence of the critical current.

In Fig. 5(a) we show the current-voltage curves of the trilayer slightly below the transition temperature while the magnetic field is increased from negative values toward positive values. A reentrant behavior is found, with an appreciable depression of superconductivity in correspondence of the $|\mathrm{AD}\rangle$ state. The critical current as a function of magnetic field (increased from negative to positive values) is shown in Fig. 5(b). The critical current in the saturated parallel state of magnetizations achieved for high negative or positive fields [$B = \pm 100$ G in Fig. 5(b)] is much larger than the critical current in $|\mathrm{AD}\rangle$ state achieved at about 30 G. Biasing the device with current in between the two critical currents, and sweeping the field up and down, the voltage vs field curve shown in Fig. 5(c) is recorded evidencing a transition from the zero-voltage state to the resistive state. The arrows in Fig. 5(c) identify the branch traced in the same magnetic-field halfloop applied to record data in Fig. 5(b).

As can be inferred from Figs. 4 and 5, biasing the device with a constant current $I_c^{|\mathrm{AD}\rangle} < I_{\mathrm{BIAS}} < I_c^{|\mathrm{PD}\rangle}$, a transition from zero-voltage state to the resistive state and vice versa can be induced at all temperatures below the critical ones during a cycle of the magnetic field. This is shown in Fig. 6(a) for our device operated at 4.2 K while biased with 7 mA. The arrows indicate a single cycle of the applied magnetic field. Depending on history, at the same magnetic field can correspond two different voltage levels. Choosing properly the bias current, these voltage levels can either be $V=0$ or $V \neq 0$ labeled as ON and OFF states in Fig. 6(a). An example of magnetic-field wave form that can be used to set the two states is shown in Fig. 6(b), where we show also the time trace of the

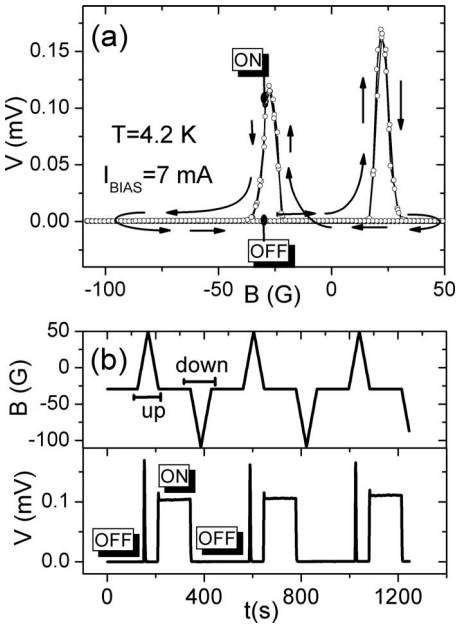

FIG. 6. (a) Voltage versus field curve during a loop of the magnetic field at 4.2 K. The biasing current is chosen in between the critical currents of the $|AD\rangle$ and $|PD\rangle$ states at the working temperature. (b) Magnetic-field wave form used to prepare the ON or OFF states together with the voltage wave form of the superconducting valve.

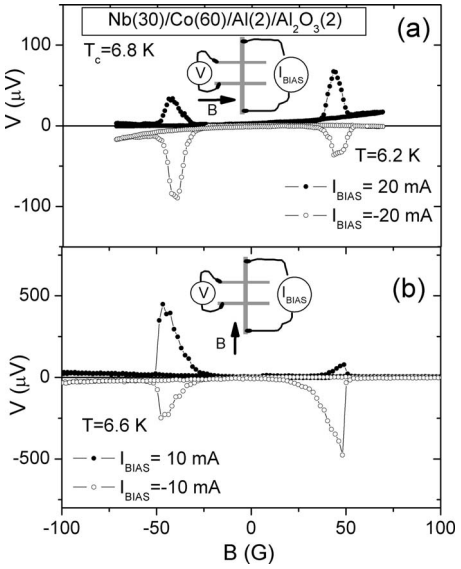

FIG. 7. Voltage versus field curve of a bilayer at positive or negative constant bias current recorded slightly below the transition temperature. The in-plane magnetic field is applied perpendicularly [Fig. 7(a)] or parallel [Fig. 7(b)] to the current direction.

voltage measured across the spin switch. The upward section of the $B(t)$ labeled *up* in Fig. 6(b) prepares the ON state, while the downward section labeled *down* prepares the OFF state. After preparation, the device stay stable in the states. In Fig. 6(b) the two states are prepared in a sequence as an example.

III. DISCUSSION

At a first glance, the superconducting valve behavior reported here could be accounted for by gap suppression[9–11,15] due to spin imbalance[16] in the $|AD\rangle$ state since the spin polarization of the metallic Co ($P \approx 0.4$) is relatively large and Nb thickness here is close to its spin-diffusion length (estimated[10] about 30 nm for Nb at cryogenic temperature). However, due to a significant component of a domain state in our $|AD\rangle$ state, the magnetoquenching can also be caused by out-of-plane field penetration (stray fields), which originated from domain walls in the domain state or during reversal of in-plane magnetization.[12–14] This mechanism, although it could also affect FS bilayers,[12,21] is found much more effective[12–14] in trilayers coherently with the rather strong magnetoresistive ratios we have observed in our trilayer structure despite the use of a quite large thickness for Nb.

Stray fields from domain walls are more effective near the coercive fields of the magnetic layers and, in fact, inspection of Figs. 2(b) and 3(b) suggests a depression of superconductivity essentially around such fields. As noticed in the discussion of Fig. 1(c), the number of domain walls (and hence stray fields) in the $|AD\rangle$ state is expected to be significantly larger than the number of domain walls in the $|PD\rangle$ state coherently with our observed magnetoquenching in the $|AD\rangle$ state. In this sense, the observed magnetoquenching can be ascribed to an amplified FS bilayer effect. To make a comparison, in Fig. 7 we show the voltage versus field curves of a Nb(30)/Co(60) bilayer capped by 2 nm Al covered by 2 nm native oxide. The curves were recorded slightly below the transition temperature, and the bias current was fixed at positive or negative values. Depression of superconductivity is observed around $B = \pm 50$ G; from AMR curves (not shown) measured slightly above the transition temperature, these are the switching fields of the magnetic layer deposited on the top of the superconductor. This is in agreement with previous results[12–14,21] on FS bilayers using different magnetic and superconducting materials. We emphasize that in bilayer samples, the switching behavior is more complicated since we now find asymmetry[14] in the peak values of the voltage but also asymmetry with respect to the current direction. Such kind of asymmetry is less evident or almost absent in the trilayer as can be seen in Figs. 2 and 5. The trilayer structure is in fact intrinsically more symmetric and effective. The stray fields act now from both sides of the sandwiched superconductor and, if the coercive fields of magnetic layers are not too different, a so-called focusing effect[12–14] can take place. Such effect, often invoked[12–14] but probably not again thoroughly described is possibly due to the domain-walls coupling across the Nb layer enhancing the local flux density in the superconductor and sharpening the switching behavior. The observation of only one voltage (resistance) peak (i.e., a not structured peak) in our trilayer [as in Figs. 5(c) and 6(a)] could be possibly explained by such a focusing effect. Moreover, due to the thickness of Nb layer, we had to put a rather thick Co layer (60 nm) in the bilayer to achieve a depression of critical current comparable to the one observed in the trilayer structure with thinner Co layers.

The amplified bilayer effect and symmetrizing effect of the trilayer structure can be better seen if we compare the

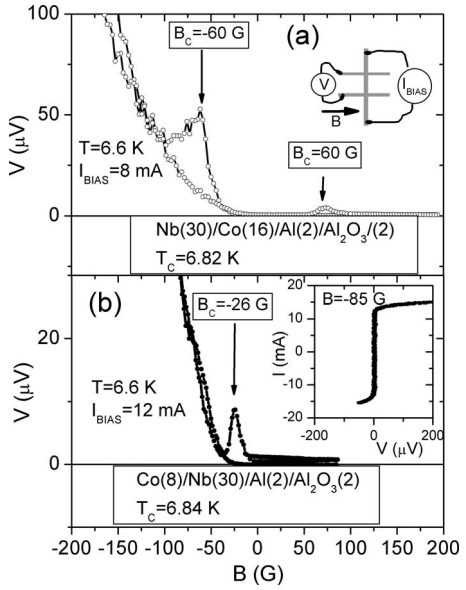

FIG. 8. (a) Voltage versus field curve of a Nb/Co bilayer at constant bias current recorded slightly below the transition temperature. The in-plane magnetic field is applied as shown in the inset. (b) Same as in (a) but for a Co/Nb bilayer. In the inset it is shown the *I-V* curve of the bilayer at a fixed field.

behavior of the Co(8)/Nb(30)/Co(16) trilayer with the behavior of the constituting bilayers Co(8)/Nb(30) and Nb(30)/Co(16). The response of these bilayers is shown in Fig. 8. A very weak magnetoquenching around coercive fields of the bilayers is observed only near the transition temperature and a strong asymmetric response is exhibited pointing to very asymmetric current voltages curve, as it is better seen in the inset of Fig. 8(b) showing the *I-V* of the Co(8)/Nb(30) at a fixed field. A comparison with Fig. 2(b) allows us to associate the larger coercive field (about 60 G) to the Co(16) grown on Nb and the lower coercive field to the Co(8) grown on the substrate. A larger coercive field despite the use of a thicker film can be explained by the different morphology induced in the Co layers by the substrate and the Nb. Moreover, the top Co layer is grown on a relatively rough Nb (estimated roughness of about 1.5 nm as noted above) that could act as pinning during reversal of magnetization thus giving larger coercive fields.

As further comment on bilayers, in Figs. 7 and 8 we observe magnetoquenching around coercive fields (due to stray fields from domain walls) as reported also in Py/Nb (Ref. 13) or MoGe/GdNi (Ref. 14) bilayers, and we have no evidence for magnetoenhancement at coercive fields as reported by other authors[21] in Py/Nb bilayers. This allows us to give a dominant role to the domain walls also in the observed magnetoquenching of the trilayer. For what concerns the asymmetric response of bilayers, we found that such asymmetry is stronger when the magnetic layer is thinner as we can see by comparison of Figs. 7 and 8. A similar strong asymmetry was observed in a MoGe/GdNi bilayer (see Fig. 6 of Ref. 14) where the sample was patterned in a narrow strip geometry as is also in our case. We can guess that the phenomenon is enhanced by size effects; but the real reason of the asymmetric response of bilayers probably deserves further study.

From the above discussion, we can associate to the stray fields from domain walls a dominant role in the suppression of superconductivity in our trilayer. For what concerns the nature of the domain walls taken into account the thickness of Co in the trilayer, we should expect Néel walls for the bottom Co layer and a combination of Néel and Bloch-wall segments (cross-tie walls) for the top layer as suggested by magnetic force microscope (MFM) studies reported[17,22,23] on Co layers of comparable thickness. Cross-tie walls are expected[23] also for the bilayer with thick Co shown in Fig. 7. Both types of walls in the ferromagnetic layers imply a local divergence of the in-plane magnetization leading to a magnetic charge that generates an out-of-plane component of the magnetic field as MFM experiments[17,22,23] and micromagnetic simulations[24] confirm.

If a second type superconductor such as Nb is involved, one can expect the formation of vortices if the out-of-plane component of magnetic field associated to domain walls exceeds the lower critical field H_{c1}. Such issue was quantitatively addressed by Burmistrov and Chtchelkatchev[25] in a FS bilayer. These authors calculated the critical value of magnetization of the magnetic layer that can induce vortices in a FS bilayer as a function of the parameters of both layers. For a given thickness of the superconducting layer (d_s), this critical magnetization can be expressed[14] as a critical minimal thickness $d_F^{\min}$ for the magnetic layer that induces vortices. Noticing that Co has very small domain-wall width ($\delta \approx 50$ nm) and a rather large saturation magnetization ($\mu_0 M_s \approx 1.6$ T), such a critical magnetic layer thickness is estimated as $d_F^{\min} \approx 6$ nm in our trilayer ($d_s = 30$ nm); so that vortex formation is expected to take place in our structure with 8- and 16-nm-thick ferromagnetic layers. Due to the use of magnetic layer thickness larger than the $d_F^{\min}$, we can also expect that stray fields from domain walls are intense enough to locally exceed the temperature-dependent upper critical field $H_{c2}(T)$, thus acting possibly also as pinning centers. Domain-walls proliferate around the coercive fields and vortex formation as well. If the Lorentz force due to the bias current becomes larger than the pinning forces, viscous vortex motion (flux flow) could take place with generation of voltage. However, from a balance of pinning forces and Lorentz and thermal forces, many regimes (flux creep, thermally activated flux flow, vortex glass, and flux flow) can occur.[26] Here the presence of two spatially disordered generators of vortices and pinning forces could induce any of these regimes and possibly a complicated mixing of them.

To gain some information on the vortex regime achieved in our magnetoquenched $|\mathrm{AD}\rangle$ state, we analyzed the behavior of current-voltage curves of the trilayer near the transition temperature. Some of these curves are shown in Fig. 9(a) on a linear scale and in Fig. 9(b) on a logarithmic scale. We found that just below the normal state fully achieved at $T_N = 4.8$ K, the curves are fitted by a simple power law $V = aI^{\alpha}$ with $\alpha = 2.2 \pm 0.1$ at $T_g = 4.62$ K and by a simple exponential law $V = bI \exp(-I_0/I)$ for $T < T_g$. Such fitting curves are shown as solid lines in Figs. 9(a) and 9(b). These curves seem to agree with the behavior predicted for a vortex-glass regime.[26–29] We were not able to obtain a comparable good fit using the simple flux creep formula[19,26] that, on the other hand, could not account for the negative curvature in the

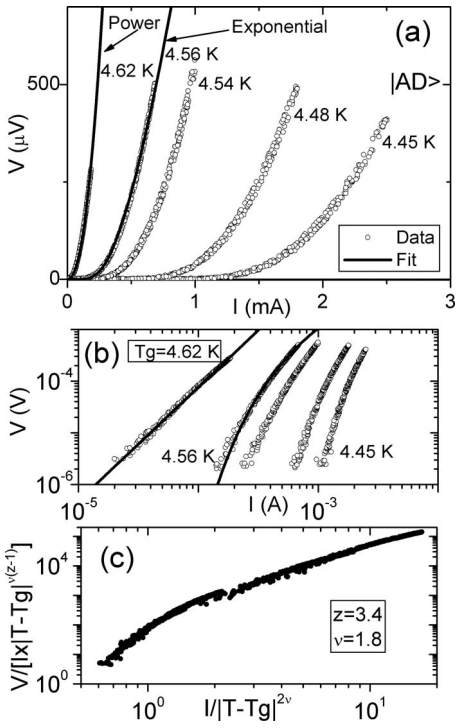

FIG. 9. (a) Current-voltage curves of the trilayer prepared in the $|\mathrm{AD}\rangle$ state recorded near the transition temperature. The solid lines are simple fitting curves. (b) Same data as in (a) represented in a logarithmic scale. (c) Scaling of the above current-voltage curves in the framework of the vortex-glass model.

$\log(V)$-$\log(I)$ curves seen in Fig. 9(b) for $T<T_g$. If a vortex-glass phase takes place, in the framework of vortex-glass model[26–29] the curves should collapse into a single one if properly scaled. This is shown in Fig. 9(c) for our data. The best scaling is achieved using the critical exponents $z=3.4\pm0.1$ [determined by the power-law exponent[26–29] $\alpha=(z+1)/2$] and $\nu=1.8\pm0.1$. These values are close to the ones reported[30] for Nb $(z=4.2, \nu=1.6)$ in the presence of homogeneous out-of-plane magnetic field though slightly lower. Nevertheless, values of critical exponents comparable to our result have been reported for some high-T_c materials,[31] particularly in the presence of an inhomogeneous distribution of pinning forces[32] as could be also in our case. We should remark that scaling of current-voltage curves below a critical temperature could be also explained in terms of a modified flux creep-flow model[33,34] in the presence of a disordered pinning forces distribution; although, the analysis is more complex from the mathematical point of view. Moreover, a clear and conclusive individuation of a vortex-glass phase should be performed analyzing many curves in a rather large range of voltage and current, which evidently is not our case. Our simple analysis only suggests that the ingredients of a vortex-glass or a flux creep-flow regime are present: a vortex lattice (i.e., a more rigid than fluid arrangement of vortices) in the presence of a disordered and inhomogeneous distribution of quite strong pinning forces. Here a thermally activated liquid vortex phase or thermally activated flux flow[26] is only achieved in a narrow range of temperatures $T_g<T<T_N$. A fluid vortex arrangement, which the Lorentz force due to the bias current could be set in a viscous motion (i.e., a flux-flow regime), could be achieved if the pinning forces were weaker. From the above discussion, this could be obtained from thinner ferromagnetic layers. In fact, we are performing preliminary experiments with thinner ferromagnetic layers both in FS and FSF structures that suggest the realization of a fully developed flux-flow regime.

We like to conclude with a comment on the meaning of resistive $(V\neq0)$ and superconducting $(V=0)$ state in the framework of our physical model based on induced vortex matter in a second type superconductor. When a second type superconductor is involved, the mixed phase between $H_{c1}(T)$ and $H_{c2}(T)$ induced by a magnetic field can be very complex[26] with a vortex matter that can have several phase transitions. A magnetic field induces Abrikosov vortices with a normal core. So, in a certain sense the mixed phase is a spatially inhomogeneous phase reverting to a truly normal phase when the vortex core size (i.e., the coherence length) diverges at $H=H_{c2}(T)$ or, if the field, is fixed at $T=T_N(H)$. In the mixed state, $V=0$ at fixed bias current means no vortex motion (i.e., pinned vortices) and $V\neq0$ means vortex motion. Therefore, when the latter case occurs as in Figs. 3(c) and 4(a), vortex phase can be present in principle up to the onset of transition, i.e., up to $T=4.8$ K in these figures. In our framework both in the $|\mathrm{PD}\rangle$ and in the $|\mathrm{AD}\rangle$ states there are domain walls and hence vortices with the difference that in the $|\mathrm{AD}\rangle$ state there are more vortices. Thus, below $T=T_N$ we are always in a mixed phase, namely, in thermally activated flux-flow regime[26] for $T_g<T<T_N$ characterized by a finite resistance $(V\neq0)$ for bias current going to zero, and in vortex-glass regime for $T<T_g$ with a zero resistance $(V=0)$ for bias current going to zero. In this sense, the difference between $V(T)$ curves of the two states extending almost up to T_N [see Fig. 4(a)] is consistent with our physical model.

IV. SUMMARY

Summarizing, we reported a superconducting valve behavior in a Co/Nb/Co trilayer at liquid-helium temperature. The parallel-domain and antiparallel-domain (magneto-quenched) states correspond to two appreciably different critical currents pointing at two slightly different critical temperatures. Biasing the device with a constant current comprised between the two critical currents, the preparation of the device in the superconductive or resistive state can be reliably achieved using weak magnetic fields. The valve behavior is compatible with the mechanism of depression of superconductivity due to the stray fields of domain walls proliferating around the coercive fields of the ferromagnetic electrodes. A simple analysis of the current-voltage curves suggests that for the relatively thick ferromagnetic layers we involved here, the stray fields induce in the superconductor a vortex matter more similar to a glassy vortex phase than to a fluid vortex phase.

*Corresponding author. giocar@sa.infn.it

[1] P. de Gennes, Phys. Lett. **23**, 10 (1966).
[2] J. J. Hauser, Phys. Rev. Lett. **23**, 374 (1969).
[3] G. Deutscher and F. Meunier, Phys. Rev. Lett. **22**, 395 (1969).
[4] A. I. Buzdin, Rev. Mod. Phys. **77**, 935 (2005).
[5] L. R. Tagirov, Phys. Rev. Lett. **83**, 2058 (1999).
[6] J. Y. Gu, C. Y. You, J. S. Jiang, J. Pearson, Ya. B. Bazaliy, and S. D. Bader, Phys. Rev. Lett. **89**, 267001 (2002).
[7] A. Potenza and C. H. Marrows, Phys. Rev. B **71**, 180503(R) (2005).
[8] Ion C. Moraru, W. P. Pratt, Jr. and Norman O. Birge, Phys. Rev. Lett. **96**, 037004 (2006); Phys. Rev. B **74**, 220507 (2006).
[9] A. Y. Rusanov, S. Habraken, and J. Aarts, Phys. Rev. B **73**, 060505(R) (2006).
[10] A. Singh, C. Sürgers, and H. v. Lohneysen, Phys. Rev. B **75**, 024513 (2007).
[11] A. Singh, C. Sürgers, R. Hoffmann, H. V. Lühneysen, T. V. Ashworth, N. Pilet, and H. J. Hug, Appl. Phys. Lett. **91**, 152504 (2007).
[12] R. Steiner and P. Ziemann, Phys. Rev. B **74**, 094504 (2006).
[13] D. Stamopoulos, E. Manios, and M. Pissas, Phys. Rev. B **75**, 184504 (2007).
[14] C. Bell, S. Tursucu, and J. Aarts, Phys. Rev. B **74**, 214520 (2006).
[15] V. Peña, Z. Sefrioui, D. Arias, C. Leon, J. Santamaria, J. L. Martinez, S. G. E. te Velthuis, and A. Hoffmann, Phys. Rev. Lett. **94**, 057002 (2005).
[16] S. Takahashi, H. Imamura, and S. Maekawa, Phys. Rev. Lett. **82**, 3911 (1999).
[17] J. Vogel, S. Cherifi, S. Pizzini, F. Romanens, J. Camarero, F. Petroff, S. Heurn, and A. Locatelli, J. Phys.: Condens. Matter **19**, 476204 (2007).
[18] A. Nemoto, Y. Otani, S. G. Kim, K. Fukamichi, O. Kitakami, and Y. Shimada, Appl. Phys. Lett. **74**, 4026 (1999).
[19] M. Tinkham, *Introduction to Superconductivity* (McGraw-Hill, Singapore, 1996).
[20] T. W. Clinton and M. Johnson, Appl. Phys. Lett. **70**, 1170 (1997).
[21] A. Yu. Rusanov, M. Hesselberth, J. Aarts, and A. I. Buzdin, Phys. Rev. Lett. **93**, 057002 (2004).
[22] M. Dreyer, M. Lohndorf, A. Wadas, and R. Wiesendanger, Appl. Phys. A: Mater. Sci. Process. **66**, S1209 (1998).
[23] M. Lohndorf, A. Wadas, H. A. M. van den Berg, and R. Wiesendanger, Appl. Phys. Lett. **68**, 3635 (1996).
[24] M. Redjdal, J. H. Giusti, M. F. Ruane, and F. B. Humphrey, IEEE Trans. Magn. **39**, 2684 (2003).
[25] I. S. Burmistrov and N. M. Chtchelkatchev, Phys. Rev. B **72**, 144520 (2005).
[26] G. Blatter, M. V. Feigelman, V. B. Geshkenbein, A. I. Larkin, and V. M. Vinokur, Rev. Mod. Phys. **66**, 1125 (1994).
[27] D. S. Fisher, M. P. A. Fisher, and D. A. Huse, Phys. Rev. B **43**, 130 (1991).
[28] R. H. Koch, V. Foglietti, W. J. Gallagher, G. Koren, A. Gupta, and M. P. A. Fisher, Phys. Rev. Lett. **63**, 1511 (1989).
[29] R. H. Koch, V. Foglietti, and M. P. A. Fisher, Phys. Rev. Lett. **64**, 2586 (1990).
[30] J. E. Villegas and J. L. Vincent, Phys. Rev. B **71**, 144522 (2005).
[31] P. L. Gammel, L. F. Schneemeyer, and D. J. Bishop, Phys. Rev. Lett. **66**, 953 (1991).
[32] M. Acosta, Víctor Sosa and C. Acosta, Revista Superficies y Vacio **12**, 12 (2001).
[33] S. N. Coppersmith, M. Inui, and P. B. Littlewood, Phys. Rev. Lett. **64**, 2585 (1990).
[34] A. N. Lykov and A. Yu. Tsvetkov, Phys. Solid State **40**, 906 (1998).